Ricerca di Sistema elettrico

# Large Eddy Simulation of a Stoichiometric Premixed CH4/Air Confined Slot Flame

D. Cecere, E. Giacomazzi, N. Arcidiacono, F.R. Picchia

LARGE EDDY SIMULATION OF A STOICHIOMETRIC PREMIXED CH4/AIR CONFINED SLOT FLAME

D. Cecere, E. Giacomazzi, N. Arcidiacono, F.R. Picchia (ENEA)

Settembre 2017

# Indice

# Sommario

Nell'ambito dello studio di cicli turbo-gas non convenzionali EGR (Exhausts Gas Recirculation) ci siamo dotati di un bruciatore denominato Romulus per comprendere gli aspetti fondamentali della combustione aria-metano in presenza di una forte concentrazione di anidride carbonica. Nel nostro apparato sperimentale, la presenza di anidride carbonica è garantita dal flusso in camera di combustione dei prodotti di combustione di due fiamme pilota di Propano.

Nella presente annualità, al fine di studiare la dinamica della combustione dell'apparato sperimentale Romulus, nella configurazione in cui il flusso di combustibile (rappresentato da $CH_4$ ed Aria) è confinato all'interno della camera di combustione in quarzo dalla forma cilindrica a sezione rettangolare, si è effettuata una Large Eddy Simulation (LES) attraverso l' utilizzo del codice proprietario HeaRT.

Il getto di combustibile fluisce ad una velocità di 17 m/s attraverso un canale rettangolare posto al centro della parte inferiore della camera di combustione. La camera di combustione ha forma di un parallelepipedo (0.03 mx0.06 mx0.25 m). Il canale di immissione del combustibile (0.003 mx0.01 m) è circondato da due piastre forate. Attraverso queste ultime vengono iniettati i gas caldi costituiti dai prodotti di combustione di una fiamma laminare stechiometrica di propano, le cui caratteristiche sono rappresentate in figura 1.2. La velocità dei gas caldi è stata calcolata in base alla portata sperimentale e risulta di 0.4 m/s. La miscela di $CH_4$/Aria, viene iniettata nella camera di combustione alla velocità di 17.7 m/s e con una fluttuazione di 2.05 m/s corrispondente ad un livello di turbolenza dell11.5%. Il numero totale di punti utilizzati nella simulazione è pari 7077888 su griglia cartesiana non uniforme ed infittita nelle tre direzioni, appena alluscita del condotto principale come mostrato nella figura 2 attraverso una slice ad x costante (x = 0). Lo schema cinetico utilizzato nella seguente simulazione presenta 17 specie chimiche differenti e 73 reazioni elementari. Le condizioni al contorno di velocità nulla e di gradiente nullo di pressione sono stati imposti sulle pareti della camera di combustione, mentre alluscita del combustore (allaltezza di z = 0.25 m) sono state imposte condizioni al contorno non riflessive. All'ingresso del condotto di immissione del combustibile le fluttuazioni di velocità sono state determinate attraverso la procedura di Klein per la produzione di turbolenza sintetica. Il numero totale di iterate è di $1.3 * 10^6$ per un tempo totale di simulazione di 0.026 s. I risultati sono stati confrontati con i dati sperimentali ottenuti nell'attività PAR:Tecnologie per l'impiantistica energetica low carbon (parte a.1, task 2).

# 1 Test case definition

The test case defined for this study consists in a confined (quartz cylinder with rectangular section) premixed slot-burner flame at atmospheric pressure. A slot-burner Bunsen configuration is especially interesting due to the presence of a mean shear in the flow. The configuration is similar to that of the experimental device already analysed in [1] but with smaller inlet dimensions (h = 3.0mm vs 25.4mm of slot width) and similar bulk velocities (17.7m/s) compared to the Filatyev experiment (3 to 12m/s). It consists of a central slot-jet of premixed reactants surrounded on both longer sides by two coflowing high temperature jets. The central slot-duct is 3. mm wide ($h$) and 10 mm long.

The central jet is a stoichiometric (equivalence ratio $\Phi = 1.0$) mixture of methane and air with a mixture temperature of 300 K. The surrounding jets have the composition and temperature of the combustion products of a laminar stoichiometric freely propagating flame of Propane. The unstrained laminar flame properties at these conditions computed using Chemkin [2] are shown in Fig. 1.1.

The central jet has a velocity of 17.7 m/s (imposed as a mean plug-flow at the inlet of the 10 mm long central duct), with a fluctuation of the 11.5%. Homogeneous isotropic turbulence is artificially generated at the inlet of the central duct by forcing a turbulent spatial correlation scale in the streamwise direction $\delta_{z,in}^{corr} = 0.4\,\text{mm}$ and a streamwise velocity fluctuation $u_z' = 2.05$ m/s used as inputs to the Klein's procedure [3] (see Table 1.2). The surrounding flows have a velocity of 0.5 m/s (imposed as a mean plug-flow) and no turbulence is forced. The actual jet Reynolds number based on the centerline streamwise velocity peak at the central duct exit and its width $h$ is $Re_{jet} = U_o h/\nu = 4000$. Other parameters characterizing the present lean premixed turbulent flame are reported in Table 1.3. These parameters locate the present flames in the Thin Reaction Zone of the combustion diagram.

The computational domain is composed of eight structured blocks (whose contours are highlighted with black lines in Fig. 1.2b) and its characteristics are summarized in Table 1.4. The domain size in the streamwise (z), crosswise (y) and spanwise (x) directions is $L_x \times L_y \times L_z = 83h \times 20h \times 10h$, $h$ being the slot width ($h = 3.0$ mm). The grid is not uniform in all the directions, it is refined in the x,y and z directions near the inlet duct walls and coarsened (upto $\Delta y \sim 1000\,\mu\text{m}$) only in the x and y directions far from the central jet at the surrounding near lateral walls, at the exit (z = 0.25 m) non reflecting boundary conditions are applied. A picture of the computational domain is shown in Fig. 1.2, where a slioce at constant x indicates the non uniformity of the grid in the y-direction.

The LES was run at atmospheric pressure using a 17 species and 73 elementary reactions kinetic mechanism [5]. Improved staggered non-reflecting inflow and outflow boundary conditions (NSCBC) were adopted at the

| Case | $\Phi$ | $T_u$ [K] | $T_b$ [K] | $S_L^{nS}$ [cm s$^{-1}$] | $\delta_L^{nS}$ [mm] |
|---|---|---|---|---|---|
| CH$_4$/$Air$ | 1.0 | 300 | 2217 | 38 | 0.430 |

Tabella 1.1: CH$_4$ − Air laminar flames characteristics based on the 23-species chemical mechanism adopted in the present LES. The apex $nS$ in the laminar flame speed and flame front thickness, respectively stand for "no Soret" effect not included in the laminar flame calculation.

| Flame | $U_{0,in}$ [m s$^{-1}$] | $T_{in}$ [K] | $u_{in}'$ [m s$^{-1}$] | $\delta_{z,in}^{corr}$ [mm] | Duct length [mm] | Duct width $h$[mm] |
|---|---|---|---|---|---|---|
| Central | 17.7 | 300 | 2.05 | 0.4 | 10. | 3.0 |
| Surrounding | 0.5 | 2227 | 0.01 | 0.1 | 4 | 10 |

Tabella 1.2: Boundary conditions imposed at the inlet of the three channels. In particular, $u_z' = u_x' = u_y'$ and $\delta_{z,in}^{corr}$, $\delta_{x,in}^{corr} = \delta_{y,in}^{corr} = \delta_{z,in}^{corr}/2$ are used as input to the Klein procedure to produce synthetic turbulence at the inlet of the three channels.
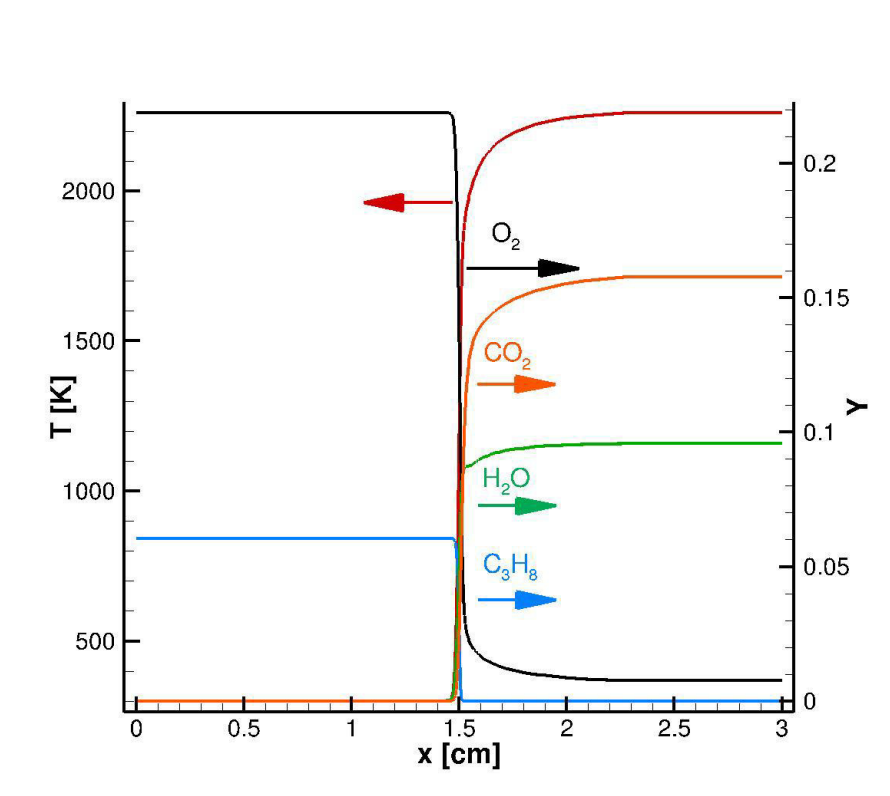
Figura 1.1: Temperature profile and major species of the stoichiometric Propane-Air flame.

| | |
|---|---|
| Jet exit velocity peak, $U_0$ [m s$^{-1}$] | 17.7 |
| Jet exit velocity fluctuation, $u'$ [m s$^{-1}$] | 2.05 |
| Jet exit turbulent length scale, $L_t$ [mm] | $\sim 3$ |
| Jet Reynolds number, $Re_{jet} = U_0 h/\nu$ | 4000 |
| Turbulent/chemical speed ratio, $u'/S_L$ | 5.54 |
| Turbulent/chemical length scale ratio, $L_t/\delta_L$ | 6.97 |
| Damkohler number, $S_L L_t/u' \delta_L$ | 12.59 |

Tabella 1.3: Actual turbulent combustion parameters characterizing the simulated $CH_4 - Air$ lean premixed flames. The turbulent velocity fluctuation and the integral length scale were evaluated at the center of the exit of the central slot-duct. The laminar flame speed and the flame front thickness were assumed as combustion parameters. The kinematic viscosity used in the calculation of the central jet Reynolds number is that of the inlet $CH_4 - Air$ mixture, $\nu \sim 5. \cdot 10^{-5}$ m$^2$ s$^{-1}$.

| | |
|---|---|
| Domain size ($L_x \times L_y \times L_z$) | $83h \times 20h \times 10h$ |
| $N_x \times N_y \times N_z$ | $220 \times 192 \times 192$ |
| Minimum grid space | $200\,\mu m$ |

Tabella 1.4: Characteristics of the computational domain. Note that $L_x$, $L_y$ and $L_z$ refer to the spanwise, crosswise and streamwise directions, respectively.
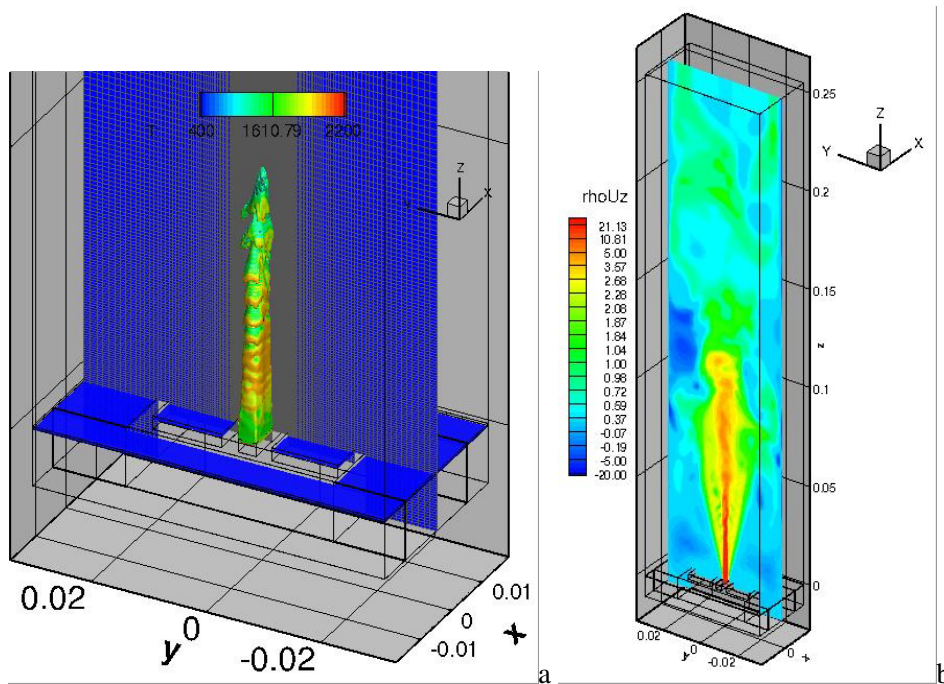
Figura 1.2: Instantaneaous HO$_2$ isosurface coloured with temperature. X-plane slice at x=0, showing the y direction grid clustering near duct's walls; b) Slice of instantaneous streamwise velocity for the Romulus burner with non-uniform computational domain.

edges of the computational domain in the x and y directions [4, 6] at the exit. The simulation was performed on the linux cluster CRESCO (Computational Center for Complex Systems) at ENEA requiring 8.5 million CPU-hours running for 70 days on 512 processors. The solution was advanced at a constant time step of $2 * 10^{-8}$ s; after the flame reached statistical stationarity, the data were collected at a frequency of 1000 Hz.

# 2 Governing Equations

Gaseous combustion is governed by a set of transport equations expressing the conservation of mass, momentum and energy, and by a thermodynamic equation of state describing the gas behaviour. For a mixture of $N_s$ ideal gases in local thermodynamic equilibrium but chemical nonequilibrium, the corresponding equations (extended Navier–Stokes equations) are:

- Transport Equation of Mass

$$\frac{\partial \rho}{\partial t} + \frac{\partial \rho u_i}{\partial x_i} = 0. \tag{2.1}$$

- Transport Equation of Momentum

$$\frac{\partial (\rho u_j)}{\partial t} + \frac{\partial (\rho u_i u_j + p\delta_{ij})}{\partial x_i} = \frac{\partial \tau_{ij}}{\partial x_i} \tag{2.2}$$

- Transport Equation of Total Energy (internal + mechanical, $\mathcal{E} + \mathcal{K}$)

$$\frac{\partial (\rho \mathcal{U})}{\partial t} + \frac{\partial (\rho u_i \mathcal{U} + p u_i)}{\partial x_i} = -\frac{\partial (q_i - u_j \tau_{ij})}{\partial x_i} \tag{2.3}$$

- Transport Equation of the $N_s$ Species Mass Fractions

$$\frac{\partial (\rho Y_n)}{\partial t} + \frac{\partial (\rho u_j Y_n)}{\partial x_i} = -\frac{\partial}{\partial x_i}(J_{n,i}) + \dot{\omega}_n \tag{2.4}$$

- Thermodynamic Equation of State

$$p = \rho \sum_{n=1}^{N_s} \frac{Y_n}{W_n} \mathcal{R}_u T \tag{2.5}$$

In the above equations, $t$ is the time variable, $\rho$ the density, $u_j$ the velocities, $\mathcal{U}$ the total energy per unit of mass, that is the sum of the internal (including chemical formation) energy, $\mathcal{E}$, and the kinetic energy, $1/2\, u_i u_i$, $p$ the pressure, $T$ the temperature, $\mathcal{R}_u$ is the universal gas constant, $W_n$ the nth-species molecular weight, $\dot{\omega}_n$ is the production/destruction rate of species $n$.

These equations are coupled to a set of constitutive equations which describe the molecular transport effects contained in the viscous stress tensor, $\tau_{ij}$, the heat flux, $q_i$, and in the diffusive mass flux, $\boldsymbol{J}_n$:

$$\tau_{ij} = 2\mu \left( S_{ij} - \frac{1}{3} S_{kk} \delta_{ij} \right) \tag{2.6}$$

$$q_i = -k \frac{\partial T}{\partial x_i} + \rho \sum_{n=1}^{N_s} h_n Y_n V_{i,n} \tag{2.7}$$

$$\boldsymbol{J}_n = \rho Y_n \boldsymbol{V}_n = -\rho Y_n \sum_{i=1}^{N_s} D_{ni}^\star \boldsymbol{d}_n - \rho Y_n D_n^T \frac{\nabla T}{T} . \tag{2.8}$$

In Eqns. (2.6)-(2.8) $\boldsymbol{S}$ is the strain rate, $\mu$ is the molecular viscosity, $k$ the termal conductivity, $\boldsymbol{V}_n$ the individual species diffusion velocity, $D_{ni}^\star$ the multicomponent Fick diffusivities, $D_n^T$ the thermal diffusivity of the $n - th$ species and $\boldsymbol{d}_n$ is the diffusional driving force [7].

In Eq. (2.7), the first term is the heat transfer by conduction, modeled by Fourier's law, the second is the heat transport due to molecular diffusion acting in multicomponent mixtures and driven by concentration gradients.

In Eq. (2.8), the diffusional driving force term $d_n$ for low-density gases is given by

$$d_n = \nabla X_n + (X_n - Y_n)\frac{\nabla p}{p} + \frac{\rho}{p}\sum_{i=1, i \neq n}^{N_s} Y_i Y_n(f_i - f_n) \,. \tag{2.9}$$

Only the first cross diffusion term of Eq. (2.9) is retained in this work, while the pressure gradient diffusion (low subsonic flame flow) and the external forces diffusion (low-density gases assumption) are neglected. Hence, according to the Hirschfelder and Curtiss [8] approximate formula for mass diffusion $V_n$ in a multicomponent mixture, and including the Soret thermo-diffusive effect, the individual species mass flux is modeled in this work as

$$J_n = -\rho\frac{W_n}{W_{mix}}D_n\nabla X_n - \rho Y_n D_n^T\frac{\nabla T}{T} \,, \tag{2.10}$$

with $X_n = Y_n W_{mix}/W_n$ and the $D_n$ is

$$D_n = \frac{1 - Y_n}{\sum_{j=1, \, j \neq n}^{N_s}\frac{X_j}{\mathcal{D}_{jn}}} \,, \tag{2.11}$$

$\mathcal{D}_{jn}$ being the binary diffusion coefficient, $D_n^T$ the n-th species thermo-diffusion coefficient, both calculated through kinetic theory.

When inexact expressions for diffusion velocities are used (as when using Hirschfelder's law), and in general when differential diffusion effects are considered, the constrain $\sum_{i=1}^{N_s} J_i = \sum_{i=1}^{N_s} \rho Y_i V_i = 0$ is not necessarily satisfied. In this paper, to impose mass conservation, an artificial diffusion velocity $V^c$ is subtracted from the flow velocity in the species transport equations [9]. This velocity, assuming Hirschfelder's law holds, becomes

$$V^c = -\sum_{n=1}^{N_s}\frac{W_n}{W_{mix}}D_n\nabla X_n \,. \tag{2.12}$$

All molecular properties for individual chemical species, except their binary mass diffusivities, are calculated a priori by using the software library provided by A. Ern (EGlib) [10, 11]. In particular, kinetic theory is used for dynamic viscosity [12, p. 23-29] and thermal conductivity [12, p. 274-278]. The calculated values are stored in a look-up table from 200 to 5000 K every 100 K. Values for intermediate temperatures are calculated at run-time by linear interpolation. Binary mass diffusion coefficients are calculated by means of kinetic theory expressions [12][p. 525-528] at run-time. The mixture-average properties are estimated by means of Wilke's formula with Bird's correction for viscosity [2, p. 14], [13], and Mathurs expression for thermal conductivity [2, p. 15], [14]. Preferential diffusion is modelled according to the Hirschfelder and Curtiss law [8].

The simulation was performed using the HeaRT code, which solves the fully compressible reactive Navier-Stokes equations (2.1)-(2.5) with the fully explicit third-order time accurate TVD Runge-Kutta scheme of Shu and Osher [15] and a sixth-order compact staggered spatial scheme for non-uniform grid (with the non uniform grid effects included in the coefficients of the compact scheme). No filter is necessary for ensuring stable solutions [16, 17, 18]. Figure 1.2b shows the computational domain adopted in the simulation with a slice indicating the non-uniform grid in the streamwise and crosswise directions (only one grid line every ten is represented), and the different stencils (due to the presence of walls and non periodic outlet) of the staggered compact scheme in the three coordinate-directions.

# 3Results

In Figure 3.1a-b-c show mean profiles of the velocity $U_z$ in the yz and xz plane respectively, and temperature in the yz plane. At $z = 0$m, at the exit of the central channel, since the flow section decreases due to the boundary layer formed inside the fuel inlet duct, the $U_z$ velocity increases with respect to the nominal input speed up to about 21 m/s. Moreover, due to the presence of the walls (at y = 0.03 m), recirculation bubbles are formed at the outlet of the fuel duct (at heights between 0 and 0.02 m), as can be seen from Figure 3a, (which shows a snapshot of the mean axial component $U_z$ velocity in the $y - z$ plane), where negative velocities of the order of 0.5 m/s are present. Figure 3.1c show the mean temperature profile in the $y - z$ plane. As can be seen, the combustion chamber is mostly filled with hot gases at a temperature of about 2200K, thanks also to the action of the large recirculating vortices that are formed on lateral sides, and only the part of volume contained inside the cone with a rectangular base of 0.003x0.01 m and height of about 0.045 m it has lower temperatures up to a minimum of 300 K (which is the temperature at which fuel is injected into the combustion chamber).
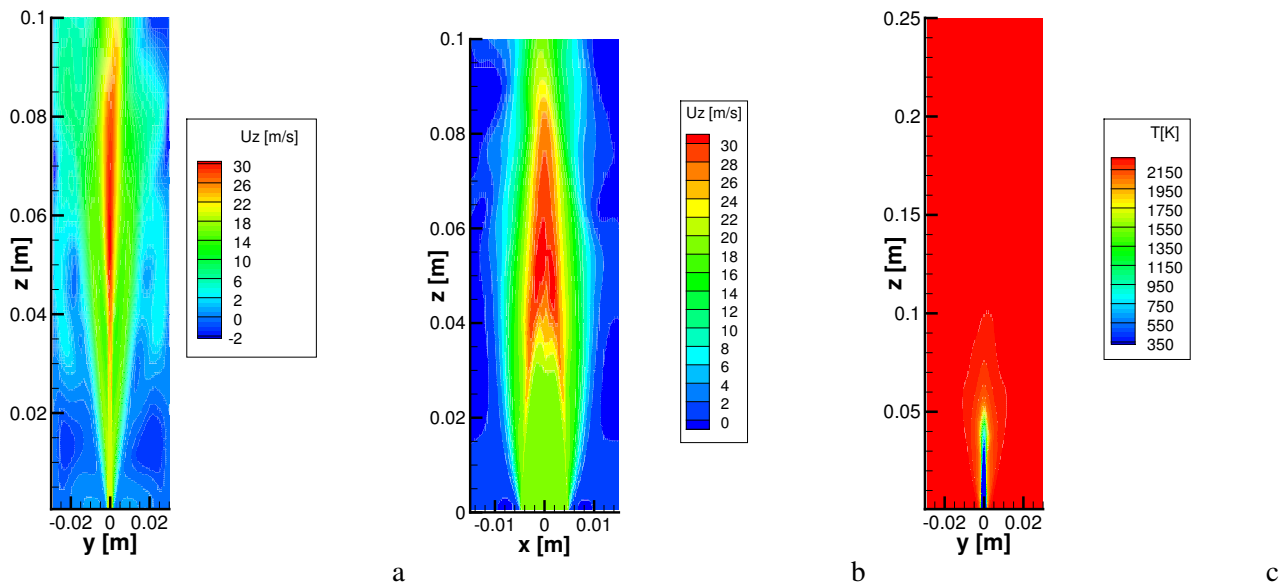


Figura 3.1: Mean $U_z$ profile in the $y - z$ plane; b) Mean $U_z$ profile in the $z - z$ plane; c) Mean temperature profile in the $y - z$ plane;.

Figure 3.2 shows comparison between experimental and numerical temperature profiles at z = 0.015 m. In the central core region (where cold premixed gases are not well mixed with hot products) and in the reaction layer (y < 0.005), the comparison is good, while, at higher y (y > 0.005) the numerical results overpredict the gas temperature of $\sim$ 150K. The combustion chamber, due to very great vortices (shown in Fig. 3.1a at z < 0.02m, see the blue region) is fillet with the hot combustion product of the stoichiometric flame (whose adiabatic temperature is $\sim 2200K$). Since, in the LES simulation we do not take into account for the heat losses due to radiative transfer (as it happens at the high difference temperature between combustion chamber and surrounding air of the experiment), the difference between the experimental and numerical temperature profiles can be expected. This suggest to include in the calculations a radiative model for heat losses.

Figures 3.3a-d show comparisons between numerical (line) and experimental (circles) streamwise velocity component.

At heights near the premixed fuel channel exit (z $\leq$ 0.015m), the $U_z$ profile is very similar to that inside the fuel channel, so statistics (after $1.2 * 10^6$ iterations and 0.026 s of simulation) are converged, hence numerical and experimental data are in very good agreement. At higher z-positions, the effects of two lateral vortices (see Figure 3.1a-b at 0.04 < z < 0.06) that have low frequencies (the velocities are of the order of $\sim 2m/s$) seems
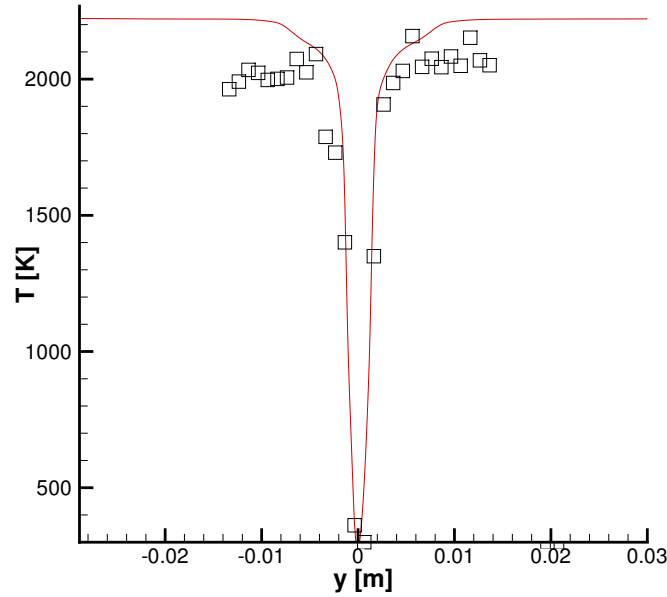
Figura 3.2: Comparison between the mean numerical (line) and experimental (squares) temperature profiles in the $y - z$ plane at $z = 0.015$ m

to be the reason for a minor agreement between numerical and experimental results. This suggest that better results can be obtained increasing the number of statistical samples in the calculation of mean velocities.

Figure 3.4 shows mean mass fraction profiles of OH and CH2O. These two intermediate radicals has their maximum value inside the flame front, for this reason we can assume that the mean height of the flame is of the order of $\sim 0.05m$.

The local geometry of the progress variable scalar field is defined by its value $c(x, t) = Y_{CO_2} + Y_{H_2O}$, its derivative in the direction normal to the iso-surface and its curvature. Flame curvatures are computed from the asymmetric tensor formed by taking the gradient of the flame front normal vector: $n_{i,j} = \partial n_i / \partial x_j$. The principal curvatures $k_1, k_2$ are the two nonzero eigenvalues of the curvature tensor $n_{i,j}$ [?]. They are related to the two nonzero invariants $I_1 = -\nabla \cdot \mathbf{n} = -(k_1 + k_2) = 2k_m$ ($k_m = I_1/2$ being the mean curvature) and $I_2 = (n_{i,i}n_{j,j} - n_{i,j}n_{j,i})/2 = k_1 k_2 = k_g$ (the Gaussian curvature) by $k_1, k_2 = \left(-I_1 \pm \sqrt{I_1^2 - 4I_2}\right)/2$. Regions having $k_g > k_m^2$ implies complex curvature and they are excluded from the statistics. Statistics of the curvature, normalized using the respective laminar flame temperature gradient thickness $\delta_L$ and accumulated on different iso-c surfaces are shown in Fig. 3.5a. Increasing the level of the reaction progress variable, the curvature peak of the Probability Distribution Function (PDF) moves towards lower negative values, although in the diffusion mixing part of the the turbulent flame structure more negative curvatures are present respect to the reaction layer.

Figures 3.5b show the mean (averaged on intervals of curvature) density weighted displacement speed $S_d^*/S_L$ and plotted against the normalized curvature $\nabla \cdot \mathbf{n}\delta_L$ at some representative values of reaction progress variable [19]. The data shown in Fig. 3.5b reveal a scatter at high values of curvature ($|\nabla \cdot \mathbf{n}\delta_L| > 5$): this is associated to the relatively low number of points in this range of curvature within the flame brush (see PDF of curvature in Fig. 3.5a) and therefore are excluded from the representation. Curvature and flame displacement speed are negatively correlated with a strong variation across the flame brush and, flame elements with negative curvatures (curvature center in the unburnt mixture) propagate with faster flame speed than positively curved elements as shown in Fig. 3.5b.

The reaction term has the strongest dependence on the location within the reaction zone as a function of the normalized curvature. In the preheat zone, the absence of chemical reactions makes the component $S_r$
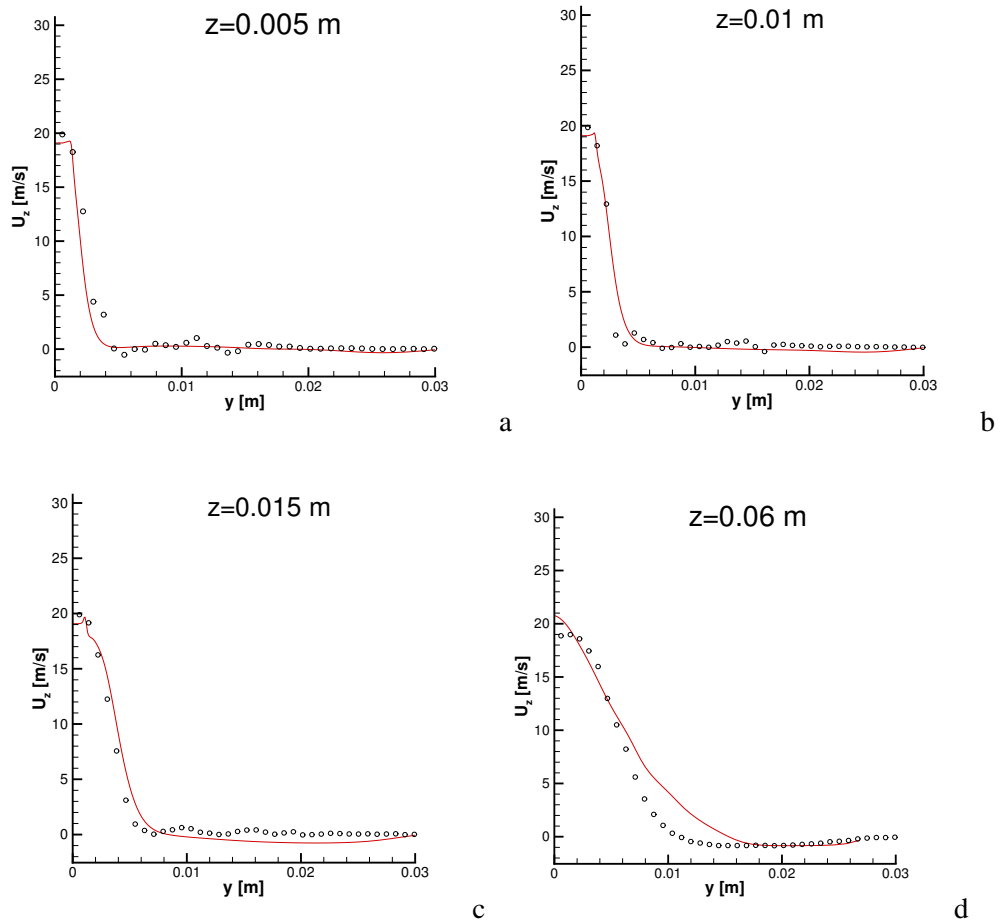
Figura 3.3: Comparison between the mean $U_z$ numerical and experimental profiles in the $y - z$ plane at a) $z = 0.005$ m; b) $z = 0.01$ m ; c) $z = 0.015$ m; d) $z = 0.06$ m.
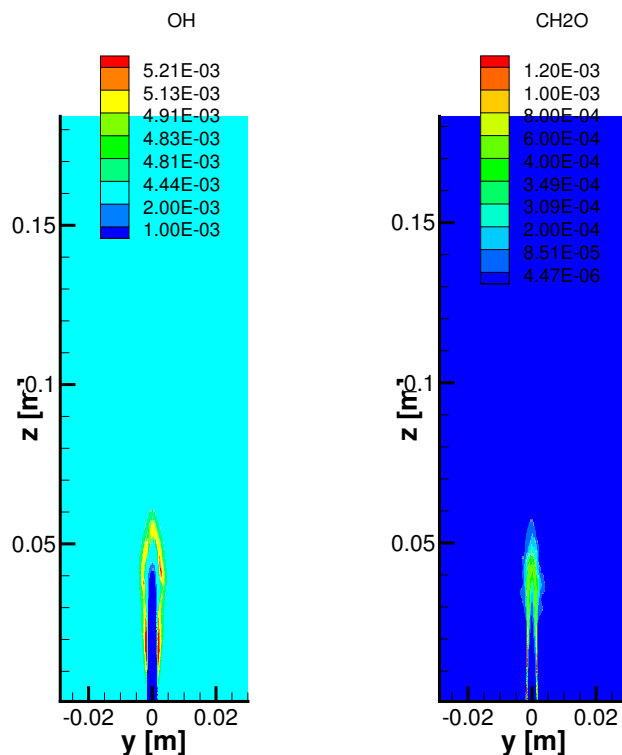
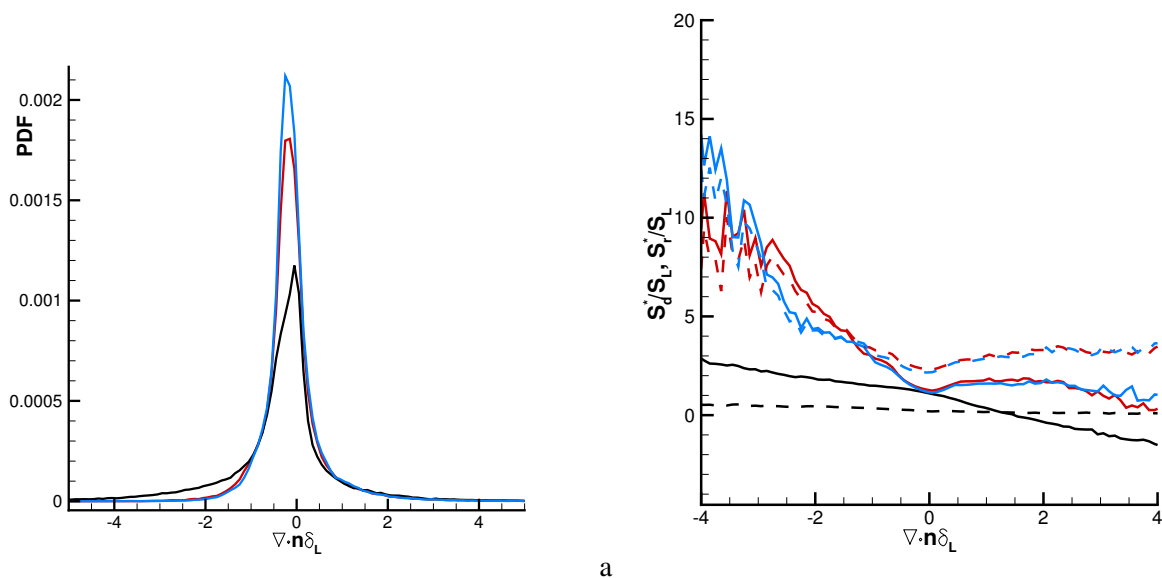Figura 3.4: Mean profiles in the y − z plane at of OH and CH2O



Figura 3.5: a) Normalized curvature of progress variable isosurface; c = 0.2 (black line), c = 0.7 (red line), c = 0.8 (blue line). b) Normalized displacement speed as a function of the curvatures and at different level of progress variable, c = 0.2 (black line), c = 0.7 (red line), c = 0.8 (blue line). Reaction component of the progress variable at different level of the progress variable (dashed line).

negligible and no correlation with curvature is observed.

# 4 Conclusions

Upon the work done in this year and described in this report, it is concluded that the Large Eddy Simulation code HeaRT is a powerful instrument to investigate complex flames as Romulus. A general description of the premixed slot flame Romulus was provided, evidencing its macroscopic characteristics by means of velocity component, curvature statistics, displacement speed as a function of curvatures and mean profiles. Numerical velocity and temperature profiles are compared with experiments. Despite the excellent agreement with the experimental results in the part of the flame near the fuel injector, due to the very slow vortical dynamics in the central part of the combustion chamber (height of 0.25m and velocity of $\sim 20\,\text{m/s}$), it is necessary to accumulate a greater number of samples in order to obtain an acceptable comparison with the experimental results in that regions.

# Bibliografia

[1] S.A. Filatyev, J.F. Driscoll, C.D. Carter, J.M. Donbar, Measured properties of turbulent premixed Flames for model assessment, including burning velocities, stretch rates, and surface densities, Combust. Flame 141, 1-21, 2005.

[2] R.J. Kee, G. Dixon-Lewis, J. Warnatz, M.E. Coltrin, Miller JA, Moffat HK, The CHEMKIN Collection III: Transport, San Diego, Reaction Design, (1998).

[3] M. Klein, A. Sadiki, J. Janicka, A digital filter based generation of inflow data for spatially developing direct numerical or large eddy simulations, J. Comput. Phys. 186, (2003), 652-665.

[4] T.J. Poinsot, S.K. Lele: Boundary Conditions for Direct Simulations of Compressible Viscous Flow. J. Comput. Phys., 101:104-129 (1992).

[5] R. Sankaran, E.R. Hawkes, J.H. Chen, T. Lu, C.K. Law, Structure of a spatially developing turbulent lean methane-air Bunsen flame, Proc. Combust. Inst. 31 (2007) 1291-1298.

[6] J.C. Sutherland , C.A. Kennedy , Improved boundary conditions for viscous, reacting, compressible Flows, J. Comput. Phys., 191:502-524, 2003

[7] E. Giacomazzi, F.R. Picchia, N.M. Arcidiacono, A Review on Chemical Diffusion, Criticism and Limits of Simplified Methods for Diffusion Coefficients Calculation, Combust. Theory Model., (2008).

[8] J.O. Hirschfelder, C.F. Curtiss, R.B. Bird, and E.L. Spotz, The Molecular Theory of Gases and Liquids (New York: John Wiley), (1954).

[9] T. Poinsot, D. Vaynante, Theoretical and numerical combustion, 2012.

[10] A. Ern and V. Giovangigli, Multicomponent Transport Algorithms, Lecture Notes in Physics, Vol. M24, Springer-Verlag, Heidelberg, 1994.

[11] A. Ern and V. Giovangigli, Fast and accurate multicomponent transport property evaluation, J. Comput. Phys. 120 (1995), pp. 105116.

[12] R.B. Bird, W.E. Stewart, E.N. Lightfoot, Transport Phenomena, Wiley International Edition, (2002).

[13] C.R. Wilke, J. Chem. Phys., 18, (1950), 517-9.

[14] S. Mathur, P.K. Tondon, S.C.Saxena, Molecular Physics, 12:569, (1967).

[15] C.W. Shu, S. Osher, Efficient implementation of essentially non-oscillatory shock-capturing schemes, J. Comput. Phys., 77, 439-471 (1988).

[16] S.K. Lele, Compact finite difference schemes with spectral like resolution, J. Comput. Phys., 103, 16-42, 1992.

[17] S. Nagarajan, S.K. Lele, J.H. Ferziger, A robust high order compact method for large eddy simulation, J. Comput. Phys., 191, 392, 2003.

[18] L. Gamet, F. Ducros, F. Nicoud, T. Poinsot, Compact finite difference scheme on non-uniform meshes. Application to direct numerical simulations of compressible flows, Int. J. Numer. Meth. Fluids, 29,159-191, 1999.

[19] D. Cecere, E. Giacomazzi, N.M. Arcidiacono, F.R. Picchia, Direct numerical simulation of a turbulent lean premixed CH4/H2Air slot flame, Combust. Flame 165 (2016) 384-401.